Fundamentals of pair diffusion in kinematic simulations of turbulence

D. R. Osborne,[1,2] J. C. Vassilicos,[1,3] K. Sung,[1] and J. D. Haigh[2]
[1]*Turbulence, Mixing and Flow Control Group, Department of Aeronautics, Imperial College London, Exhibition Road, London SW7 2BY, United Kingdom*
[2]*Space & Atmospheric Physics, Department of Physics, Imperial College London, Exhibition Road, London SW7 2BY, United Kingdom*
[3]*Institute for Mathematical Science, Imperial College London, Exhibition Road, London SW7 2BY, United Kingdom*
(Received 5 October 2005; revised manuscript received 20 March 2006; published 27 September 2006)

We demonstrate that kinematic simulation (KS) of three-dimensional homogeneous turbulence produces fluid element pair statistics in agreement with the predictions of L F. Richardson [Proc. R. Soc. London, Ser. A **110**, 709 (1926)] even though KS lacks explicit modeling of turbulent sweeping of small eddies by large ones. This scaling is most clearly evident in the turbulent diffusivity's dependence on rms pair separation and, to a lesser extent, on the pair's travel time statistics. It is also shown that kinematic simulation generates a probability density function of pair separation which is in good agreement with recent theory [S. Goto and J. C. Vassilicos, New J. Phys. **6**, 65 (2004)] and with the scaling of the rms pair separation predicted by L. F. Richardson [Proc. R. Soc. London, Ser. A **110**, 709 (1926)]. Finally, the statistical persistence hypothesis (SPH) is formulated mathematically and its validity tested in KS. This formulation introduces the concept of stagnation point velocities and relates these to fluid accelerations. The scaling of accelerations found in kinematic simulation supports the SPH, even though KS does not generate a Kolmogorov scaling for the acceleration variance (except for a specific case and a limited range of outer to inner length-scale ratios). An argument is then presented that suggests that the stagnation points in homogeneous isotropic turbulence are on average long-lived.

DOI: 10.1103/PhysRevE.74.036309 PACS number(s): 47.27.T−, 47.27.Gs, 47.27.tb, 92.10.Lq

I. INTRODUCTION

A. Searching for Richardson's dispersion laws in turbulent flows

Richardson [1] made the first quantitative prediction relevant to inertial-range turbulence when he proposed the locality-in-scale hypothesis and derived the "four-thirds" law for diffusion in isotropic turbulence,

$$\frac{d}{dt}\langle\Delta^2(t)\rangle \sim \langle\Delta^2\rangle^{2/3}, \tag{1}$$

where Δ is the separation of the two fluid elements.

Many years later, two independent studies [2,3] applied similarity theory [4] to the locality-in-scale hypothesis and obtained Eq. (1), which, when integrated, gives the temporal scaling of

$$\langle\Delta^2(t)\rangle \sim \epsilon t^3 \tag{2}$$

in the inertial range.

Understandably there has been much interest in verifying these relations both experimentally and numerically. Experimental studies are notoriously difficult due to the need to capture Lagrangian statistics of two neutral marker particles simultaneously in the same turbulent flow. Nevertheless, recent laboratory experiments [5,6] have claimed significant ranges of $\langle\Delta^2(t)\rangle \sim t^3$ in two- and three-dimensional turbulence, respectively, despite having limited Reynolds numbers, R_λ of around 100 (the Reynolds number is not reported in Ref. [5] so we take the value reported for an identical experimental setup [7]). However, there are doubts as to whether these laboratory experiments really do observe a t^3 regime or merely a low-Reynolds-number transitional regime that is locally approximated by a t^3 growth.

Direct Numerical Simulation (DNS) experiments are also faced with the difficulty of simulating Reynolds numbers that could be considered high enough for purely inertial-range statistics to be produced. References [8–10] simulated relative dispersion in a turbulent flow with an R_λ comparable to the experimental values. While Ref. [8] cautiously reported some evidence of a t^3 regime over a time range so small that such caution was fully justified, Refs. [9,10] presented evidence that spurious t^3 regimes can result from strong dependencies on initial conditions. Reference [11], taking advantage of more powerful computing resources, simulated relative diffusion in a flow with $R_\lambda = 283$ and reported a t^3 regime although, again, the results were highly dependent on the initial separation of the particle pair throughout the power-law range, which should not be the case in an authentic t^3 regime. However, these simulations remain some way from the extremely high Reynolds numbers required to capture pair-diffusion statistics and mechanisms, so other techniques must also be used to further investigate pair dispersion.

Synthetic turbulence and, more specifically, kinematic simulation (KS), has been used in numerous studies of relative turbulent diffusion. Velocity fields constructed from stream functions built from radial octaves impose an energy spectrum, $E(k) \sim k^{-5/3}$, onto the field and observe a clear Richardson t^3 regime [12]. Hitherto, studies involving KS (see Sec. I B for a full description of the model) have presented Richardson ranges of $\langle\Delta^2(t)\rangle \sim t^3$ spanning more than a decade for two-dimensional simulations [13]. Three-dimensional studies [14] present evidence showing that Eq.

(1) is verified over a significant range of scales. Recently, however, it has been proposed [15] that the KS model's lack of sweeping (see Sec. II A) should imply

$$\frac{d}{dt}\langle \Delta^2(t)\rangle \sim \langle \Delta^2\rangle^{7/9}, \tag{3}$$

instead of Eq. (1) and a corresponding $\langle \Delta^2(t)\rangle \sim \epsilon t^{9/2}$ behavior in the inertial range. These authors [15] also present KS evidence to that effect.

Therefore in the first half of this paper we investigate the temporal scaling of the mean-square separation in three-dimensional KS and show that neither a t^3 nor a $t^{9/2}$ scaling region is clearly observed. The differences between this and previous KS studies on the one hand and the KS study of Ref. [15] on the other are investigated in terms of the turbulent diffusivity, $\frac{d}{dt}\langle \Delta^2(t)\rangle$, and the time step of integration. It is shown that the difference in computational resources of the two studies is not a significant factor but that the numerics of the latter study [15] may favor their theoretical argument. We corroborate the previous three-dimensional result [14], that, in spite of the absence of sweeping in kinematic simulation, Eq. (1) holds rather than Eq. (3) and ask whether an approach based on the principle of straining stagnation points [17] might account for the validity of Eq. (1) in KS. This leads us to study the entire probability distribution function (PDF) of $\Delta \equiv |\mathbf{\Delta}|$ in kinematic simulation as well as the scalings of exit times [12]. On the basis of a generalized PDF equation [17] we establish a relation between $\langle \Delta^2(t)\rangle$ and the average travel time a fluid element pair takes to separate from its initial condition to some specified threshold. Finally, we introduce a quantitative formulation of the statistical persistence hypothesis [17,18] (SPH) and we use this formulation to demonstrate the validity of this hypothesis in Kolmogorov turbulence, and to determine its validity in KS.

B. Kinematic simulation

Kinematic simulation (KS) is a method for simulating Lagrangian statistics and turbulent diffusion properties. KS is based on a kinematically obtained Eulerian velocity field that is incompressible and consistent with Eulerian statistics up to the second order, such as the energy spectrum $E(k)$ in wave-number space. There is no assumption of Markovianity at any level. Instead, a persistence parameter λ controls the degree of unsteadiness of the turbulence. It is worth mentioning that when the prescribed energy spectrum has the form $E(k) \sim k^{-5/3}$ the model is in good agreement with laboratory experiments for two-particle statistics [14], three-particle statistics [19], and concentration variances [20] (the term "particle" that is used here is interchangeable with "fluid element"). KS is also in good agreement with DNS for two-particle statistics [21].

The flow velocity at a point $\mathbf{x}$ and a time t is constructed, in the case of homogeneous turbulence, by the summation of independent, randomly orientated, Fourier modes. These modes represent the contribution of a finite number of turbulent modes in the inertial range of the Eulerian energy spectrum. Hence kinematic simulation should only model the flow field in a qualitative and highly reduced sense. What is not modeled in kinematic simulation are the phase correlations between Fourier modes, their interactions, and their dynamics. Lagrangian statistics are achieved by synthesizing physical space only along particle trajectories.

The formulation of the velocity field used in this study follows from more recent kinematic simulation studies [13,20]. The KS velocity field is kinematically prescribed to be

$$\mathbf{u}(\mathbf{x},t) = \sum_{n=0}^{N_k} \mathbf{a_n}\cos(\mathbf{k_n}\cdot\mathbf{x} + \omega_n t) + \mathbf{b_n}\sin(\mathbf{k_n}\cdot\mathbf{x} + \omega_n t), \tag{4}$$

where N_k is the total number of representative Fourier modes, $\mathbf{a_n}$ and $\mathbf{b_n}$ are the decomposition coefficients corresponding to the wave vector $\mathbf{k_n}$ and ω_n is the unsteadiness frequency.

The wave vector

$$\mathbf{k_n} = k_n \hat{\mathbf{k}}_\mathbf{n} \tag{5}$$

is randomly orientated by a random choice of the unit vector $\hat{\mathbf{k}}_\mathbf{n}$. The wave numbers are distributed via

$$k_n = k_1 \left(\frac{k_{N_k}}{k_1}\right)^{(n-1)/(N_k-1)}, \tag{6}$$

with n an integer such that $1 \le n \le N_k$. Reference [18] found that this wave number distribution results in the quickest convergence of the Lagrangian statistics.

To ensure that the Fourier modes' orientations are random and the velocity field still satisfies incompressibility, the orientations of $\mathbf{a_n}$ and $\mathbf{b_n}$ are chosen independently and randomly in a plane normal to $\mathbf{k_n}$, i.e.,

$$\mathbf{a_n}\cdot\mathbf{k_n} = \mathbf{b_n}\cdot\mathbf{k_n} = 0. \tag{7}$$

Furthermore, magnitudes of $\mathbf{a_n}$ and $\mathbf{b_n}$ are chosen to conform with the prescribed energy spectrum $E(k)$, i.e.,

$$|\mathbf{a_n}|^2 = |\mathbf{b_n}|^2 = 2E(k_n) \triangle k_n, \tag{8}$$

where

$$\Delta k_n = \begin{cases} \dfrac{k_2 - k_1}{2} & n = 1 \\ \dfrac{k_{n+1} - k_{n-1}}{2} & n \in [2, N_k - 1] \\ \dfrac{k_{N_k} - k_{N_k-1}}{2} & n = N_k \end{cases}. \tag{9}$$

The Eulerian energy spectrum $E(k)$ is the main input in kinematic simulation of homogeneous isotropic turbulence (along with a coefficient of the unsteadiness frequency as we see later on in this section). The inertial range form of the energy spectrum [4] is

$$E(k) = C_K \epsilon^{2/3} k^{-5/3}, \tag{10}$$

where ϵ is the rate of dissipation of kinetic energy per unit mass and C_K is the Kolmogorov universal constant. In this study, KS only models the inertial range of the spectrum

unless explicitly stated; hence k is within the surrogate inertial range, $k_1<k<k_\eta$ where $k_\eta \equiv k_{N_k}$. We use the term "surrogate" to indicate that, in KS, the range $k_1<k<k_\eta$ is not dynamically inertial but simply the range over which the K41 spectrum [4] is prescribed to hold.

It is also the purpose of this study to consider departures from Kolmogorov's $-\frac{5}{3}$ law, either as a reflection of intermittency or for the purpose of experimenting with the dependence of various Lagrangian statistics [13,22,23] on the scaling of $E(k)$. We therefore write the general form of the energy spectrum

$$E(k) = C_T u_{rms}^2 L(kL)^{-p}, \tag{11}$$

where $L=\frac{2\pi}{k_1}$ and $p>1$ to ensure that there is no infinite energy at the small scales when k_η is taken to infinity. The dimensionless constant $C_T=C_T(p,k_1,k_\eta)$ is such that

$$\frac{3u_{rms}^2}{2} = \int_{2\pi/L}^{2\pi/\eta} E(k)dk, \tag{12}$$

where $\eta=\frac{2\pi}{k_\eta}$. The form [Eq. (11)] of the spectrum is unambiguous in KS where turbulence dynamics are absent and therefore ϵ is not directly defined. However, by using the cornerstone turbulence relation [24]

$$\epsilon = C_\epsilon \frac{u_{rms}^3}{L}, \tag{13}$$

where C_ϵ is a dimensionless constant, Eq. (11) reduces to Eq. (10) for $p=-\frac{5}{3}$ when $C_K C_\epsilon^{2/3}=C_T$.

Unless otherwise explicitly stated, the value of p is set to $\frac{5}{3}$ in this study. The value of C_ϵ does not need to be set as an input in our simulation and it should not be expected to be equal to corresponding values published in the literature as L is not the integral length scale (which, however, scales with L).

Time dependence is introduced via an "unsteadiness frequency" ω_n, which we take to be proportional to the eddy turnover frequency of the mode n,

$$\omega_n = \lambda\sqrt{k_n^3 E(k_n)}, \tag{14}$$

where λ is the "unsteadiness" or "persistence" parameter which, as will be seen in later sections, can have a significant effect on one-particle two-time Lagrangian statistics [13,22,23]. In Sec. III we experiment both with Eq. (14) and with

$$\omega_n = \lambda u_{rms} k_n. \tag{15}$$

Values of λ equal to, or very close to, zero generate velocity fields that are frozen, or approximately frozen in time, i.e., a velocity field with infinite, or near-infinite, persistence in time. The other extreme of very large values of λ generates extremely unsteady velocity fields with very fast time variations and very little persistence of flow structure.

II. TURBULENT PAIR DIFFUSIVITY AND SEPARATIONS IN KINEMATIC SIMULATIONS

A. Absence of sweeping of small scales by larger scales in kinematic simulation

Kinematic simulation does not model the advection of small-scale eddies by large energy-containing motions [25] due to the independent nature of the Fourier modes. This problem has been found to significantly affect the properties of the one-particle Lagrangian statistics extracted from the model [26] and it has been recently argued by Thomson and Devenish [15] that relative dispersion, i.e., two-particle statistics, could also be affected and it is felt that it would be useful to outline their arguments in this section.

The rate of mean-square separation, or eddy diffusivity, might be expressed in terms of a characteristic relative velocity δV between fluid element pairs and a time scale τ over which such relative velocities change. Both δV and τ are functions of the mean-square separation $\langle\Delta^2(t)\rangle$ and

$$\frac{d}{dt}\langle\Delta^2(t)\rangle \sim \delta V^2 \tau. \tag{16}$$

Classically, the relative velocity δV obeys Kolmogorov scaling and $\delta V^2 \sim (\epsilon\langle\Delta^2\rangle^{1/2})^{2/3}$. The time scale τ, often referred to as the eddy decorrelation time, obeys similar scaling properties provided the small eddies are swept with the fluid element by the larger eddies [25]. Hence

$$\tau \sim \epsilon^{-1/3}\langle\Delta^2\rangle^{1/3}. \tag{17}$$

Substituting back into the diffusivity equation [Eq. (16)] we recover Richardson's law,

$$\frac{d}{dt}\langle\Delta^2(t)\rangle \sim \epsilon^{1/3}\langle\Delta^2(t)\rangle^{2/3}, \tag{18}$$

which implies that $\langle\Delta^2(t)\rangle \sim t^3$ for $\max(\eta,\Delta_0) \ll \langle\Delta^2\rangle^{1/2} \ll L$, where $\Delta_0 \equiv \Delta(t=0)$.

Without the sweeping of the small eddies by the larger ones, fluid elements are rapidly advected by the large eddies *through* the small eddies and so another time scale becomes important. Then, as argued in Ref. [15], the eddy decorrelation time becomes of the order of the time it takes the local flow velocity to sweep the particles through the eddy, i.e.,

$$\tau \sim \frac{\langle\Delta^2\rangle^{1/2}}{u'}, \tag{19}$$

where u' is the rms turbulence velocity (averaged over the pairs' Lagrangian trajectories and therefore equal to the root-mean-square velocity of the Eulerian field, u_{rms}, in homogeneous turbulence [27]). This leads to the diffusivity

$$\frac{d}{dt}\langle\Delta^2(t)\rangle \sim \frac{\epsilon^{2/3}\langle\Delta^2\rangle^{5/6}(t)}{u'}, \tag{20}$$

the integration of which leads to

$$\langle\Delta^2(t)\rangle \sim \frac{\epsilon^4 t^6}{u'^6} \tag{21}$$

for $\max(\eta,\Delta_0) \ll \langle\Delta^2\rangle^{1/2} \ll L$.

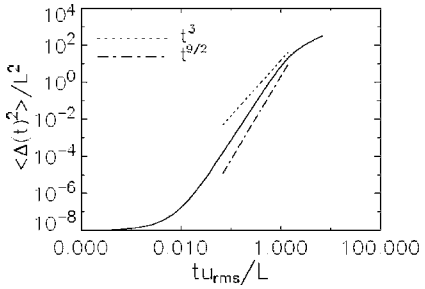

FIG. 1. Particle pair mean-square separation $\langle\Delta^2(t)\rangle$, normalized with the large scales. No t^3 or $t^{9/2}$ scaling is observed. Flow parameters are as in Table I. Initial separation $\Delta_0=0.1\eta$. Unsteadiness frequency $\omega_n=\lambda\sqrt{k_n^3E(k_n)}$.

Thomson and Devenish [15] refine their argument by distinguishing between different ensembles of pairs which experience different values of u' as would result from averages taken over their different histories (in which case there is a distribution of values of u', most of which deviate from u_{rms}). They introduce mean-square separations conditional on u', i.e., $\langle\Delta^2\rangle_{u'}$, so that

$$\langle\Delta^2\rangle=\int_0^\infty du'p(u')\langle\Delta^2\rangle_{u'}, \tag{22}$$

where $p(u')$ is the probability density function of the rms turbulence velocity u'. Recognizing that when u' is small enough the sweeping problem is absent and therefore $\langle\Delta^2\rangle_{u'}\sim\epsilon t^3$ applies, whereas when u' is large enough, $\langle\Delta^2\rangle_{u'}$ is sweeping-dominated so that $\langle\Delta^2(t)\rangle\sim\frac{\epsilon^4t^6}{u'}$ applies, they estimate a velocity which divides these two regimes, that is, when $\epsilon t^3\sim\frac{\epsilon^4t^6}{u'^6}$, which leads to $u'\sim\sqrt{\epsilon t}$. Hence

$$\langle\Delta^2\rangle\sim\int_0^{\sqrt{\epsilon t}}\epsilon t^3p(u')du'+\int_{\sqrt{\epsilon t}}^\infty\frac{\epsilon^4t^6}{u'^6}p(u')du', \tag{23}$$

and using a Gaussian form for $p(u')$ with a standard deviation of u_{rms}, they obtain

$$\langle\Delta^2(t)\rangle\sim\frac{\epsilon^{5/2}t^{9/2}}{u_{rms}^2}. \tag{24}$$

This translates into an overall mean diffusivity contribution of

$$\frac{d}{dt}\langle\Delta^2(t)\rangle\sim\langle\Delta^2\rangle^{7/9}. \tag{25}$$

B. Kinematic simulation results for mean-square separation and mean diffusivity

Due to the questions over kinematic simulation's ability to reproduce the appropriate scalings for the relative dispersion of a particle pair and, in particular, the obvious disagreement between other KS studies [13,14,22] and Ref. [15], it would seem appropriate to start by using KS to calculate $\langle\Delta^2(t)\rangle$. Typical results are depicted in Fig. 1 and the flow parameters are presented in Table I; the initial separation between the fluid element pair Δ_0 is 0.1η. The value of the persistence parameter is chosen as $\lambda=0.5$ [22,14]. Looking at Fig. 1 neither a regime of $\langle\Delta^2(t)\rangle\sim\epsilon t^3$ nor one of $\langle\Delta^2(t)\rangle\sim\epsilon t^{9/2}$ is clearly observed, even though the ratio of outer to inner turbulent length scales, $\frac{L}{\eta}$, is 10^4 and therefore unusually large. $\langle\Delta^2(t)\rangle$ is known to heavily depend on the initial separation Δ_0 in kinematic simulations over most of the inertial range when $\Delta_0<\eta$, even for extremely large values of $\frac{L}{\eta}$ [14,28]. This strong Δ_0 dependence has now also been observed in laboratory experiment [16]. This dependence therefore interferes with the time dependency and hence masks it. For $\Delta_0=\eta$, however, we do find $\langle\Delta^2(t)\rangle\sim\epsilon t^3$ over an extended range of scales as reported in Fig. 7.

TABLE I. Run specification for the Richardson pair separation experiment. N_R is the number of KS flow field realizations and N_p is the number of sample trajectories per realization. The Kolmogorov time scale $t_\eta=\epsilon^{-1/3}k_\eta^{-2/3}$. The turbulent energy dissipation rate ϵ is determined by Eq. (13).

$k_1=\frac{2\pi}{L}$ $(2\pi\ \mathrm{m}^{-1})$	$k_\eta=\frac{2\pi}{\eta}$ $(2\pi\ \mathrm{m}^{-1})$	N_k	u_{rms} $(\mathrm{m\ s}^{-1})$	λ	Δt (s)	N_R	N_p
1.0	10000.0	100	1.0	0.5	$0.01t_\eta$	100	100

To minimize this initial separation dependency it has been argued that Eq. (1) should be calculated directly [14]; this is easily obtainable in numerical studies yet still presents a significant challenge for experimentalists despite the increased availability of Lagrangian differential quantities [29–32]. We present the directly calculated diffusivity results for KS in Fig. 2 for initial separations of $\Delta_0=0.1\eta$ and $\Delta_0=\eta$.

It is obvious that there is still some residual dependence on the initial separation. However, a power law is found over a significant range of scales with three-quarters ($\Delta_0=0.1\eta$) to one-half ($\Delta_0=\eta$) of the inertial range exhibiting the Richardson $\langle\Delta^2(t)\rangle^{2/3}$ behavior. This is an overwhelming improvement on Fig. 1, where no correct t^3 scaling nor $t^{9/2}$ scaling was observed over the temporal inertial range.

The results of Fig. 2 are in stark contrast to those of Thomson and Devenish [15], who find strong $t^{9/2}$ scaling for the mean-square separation over ranges up to two decades of the temporal inertial range and so presumably find the appropriate form of diffusivity [Eq. (25)] although they do not present it. In Fig. 2 we present in the inset figure the compensated curves for the case where $\Delta_0=0.1\eta$ corresponding to diffusivities $\frac{d}{dt}(\langle\Delta^2(t)\rangle)\sim\Delta^{4/3}$ and $\frac{d}{dt}(\langle\Delta^2(t)\rangle)\sim\Delta^{14/9}$, respectively, in an attempt to distinguish between the two scaling values. Clearly the Richardson scaling remains a more convincing candidate with strong inertial range power law. Furthermore, this scaling is surprisingly robust as it survives even if we decimate the number of modes in KS further to, say, $N_K=10$ (see Fig. 3). With such differences in the results it is worth examining the main difference between the simulations of Ref. [15] and those of this study and other cited papers, namely, the time step used for Lagrangian integrations.

C. Time step

The major difference between the two studies is the implementation of the integration time step. This study uses

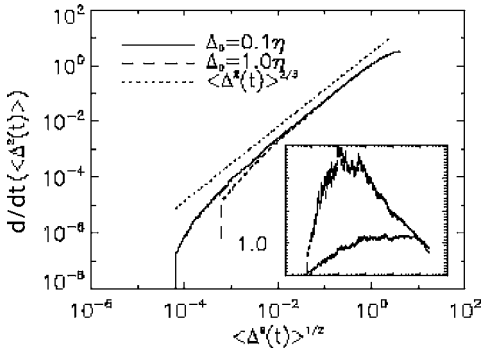

FIG. 2. Evolution of particle pair mean-square separation rate $\frac{d}{dt}[\langle\Delta^2(t)\rangle]$ with pair separation $\langle\Delta^2(t)\rangle^{1/2}$. Dependency on initial conditions is significant but less than that for Figs. 1 and 7 and the expected scaling $\langle\Delta^2(t)\rangle^{2/3}$ is found in the inertial range for both choices of Δ_0 (flow parameters are detailed in Table I). The inset depicts the solid curve in the main plot ($\Delta_0=0.1\,\eta$) compensated by $\Delta^{4/3}$ (lower solid line) and $\Delta^{14/9}$ (upper dashed line); note that the y axis of the inset figure is linear. Unsteadiness frequency $\omega_n=\lambda\sqrt{k_n^3E(k_n)}$.

a constant time step, $\Delta t=0.01\tau_\eta$, where τ_η is the Kolmogorov time scale. Hence $\Delta t\ll\tau_\eta$ and we have checked that, in all the cases studied here, it is also at least an order of magnitude smaller than the sweeping time scale $\frac{\eta}{u_{rms}}$. However, Thomson and Devenish [15] use an adaptive time step of the form

$$\Delta t=\min\left(C_1\frac{\min(\Delta,L)}{u_{rms}},C_2\frac{[\min(\Delta,L)]^{2/3}}{\lambda\epsilon^{1/3}}\right). \tag{26}$$

C_1 and C_2 are constants that are given the values 0.1 and 0.01, respectively, by Ref. [15]. Note that this adaptive time step depends on the instantaneous separation of the particles and so is often larger than the smaller time scales in the flow. Note also that it is adapted to the expected mix of average sweeping and inertial time scales that the argument of Ref. [15] is built on and that it increases, on average with time.

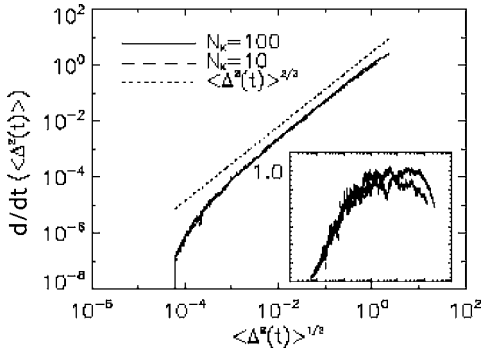

FIG. 3. Evolution of particle pair mean-square separation rate $\frac{d}{dt}[\langle\Delta^2(t)\rangle]$ with pair separation $\langle\Delta^2(t)\rangle^{1/2}$. Initial separation $\Delta_0=0.1\,\eta$. Dependency on the number of modes N_K (all other flow parameters as in Table I) used in the simulation is extremely small when looking for the scaling $\langle\Delta^2(t)\rangle^{2/3}$. The inset depicts the compensated curve; note that the y axis of the inset figure is linear. Unsteadiness frequency $\omega_n=\lambda\sqrt{k_n^3E(k_n)}$.

The constant time step is all-resolving and devoid of such adaptive assumptions. We replace our constant time step with this adaptive time step and perform an identical simulation to that specified in Table I. The result is presented in Fig. 4. (Thomson and Devenish [15] addressed the issue concerning the validity of their adaptive time step, albeit inconclusively.)

It is also clear that the adaptive time step underestimates the mean-square separation from quite early on, and that this underestimation becomes particularly severe at times comparable to and larger than L/u_{rms}. The adaptive time step is effectively constant at large scales (comparable to L) where it scales as L/u_{rms} and can therefore be unacceptably large. With such a large time step it might not be surprising to find large deviations from the mean-square separation calculated by integrating with a constant all-resolving time step as we do in the case presented here. However, the range of validity of the adaptive time step as a function of the parameters C_1 and C_2 on which it depends, integration time, initial separation, unsteadiness parameter λ, and other parameters of the velocity field would require a full study of its own and is beyond the scope of this paper. Nevertheless, we can conclude that the adaptive time step chosen in Ref. [15] does not reproduce the correct behavior in the case of Fig. 4 and that it may therefore be responsible for some of the different KS results obtained in Ref. [15] compared with all other kinematic simulation studies, including this one (we guess that in some way the adaptive time step "misses out" the persistent part of the flow; a feature that we explore in the following sections). We therefore can also conclude that KS reproduces Richardson's law [1] [Eq. (1)]. As discussed by previous authors [14,28], however, the resulting t^3 dependence of $\langle\Delta^2\rangle$ is not so clear due to strong dependence on the initial separation Δ_0, which masks the time dependence.

III. TURBULENT PAIR DIFFUSION AND STRAINING STAGNATION POINTS

A. Probability distribution function

Kinematic simulation results do not support the eddy diffusivity approach of Ref. [15], which is based on the idea that the separation of two particles in a flow is an inherently *continuous* process. However, to describe the mechanism of pair separation in KS we may, perhaps, utilize an alternative view grounded in the notion that it is the spatial distribution of straining stagnation points and the discontinuous series of sudden separation events that such points cause, which facilitates the observed algebraic separation growth [13,22,17,34]. DNS of two-dimensional (2D) inverse cascading turbulence [17] and laboratory experiments in 2D and 3D turbulence [5,6] have produced compelling evidence of pair trajectories which travel together for significant durations and then separate suddenly. We now present a summary of this approach and then use kinematic simulations to interrogate it.

In this approach, fluid element pairs with an initial separation Δ_0 will travel together following streamlines at an approximately constant separation until encountering an "event" in the flow where the separation is abruptly increased by a factor ρ_{ph} that is greater than 1, i.e., $\Delta=\rho_{ph}\Delta_0$.

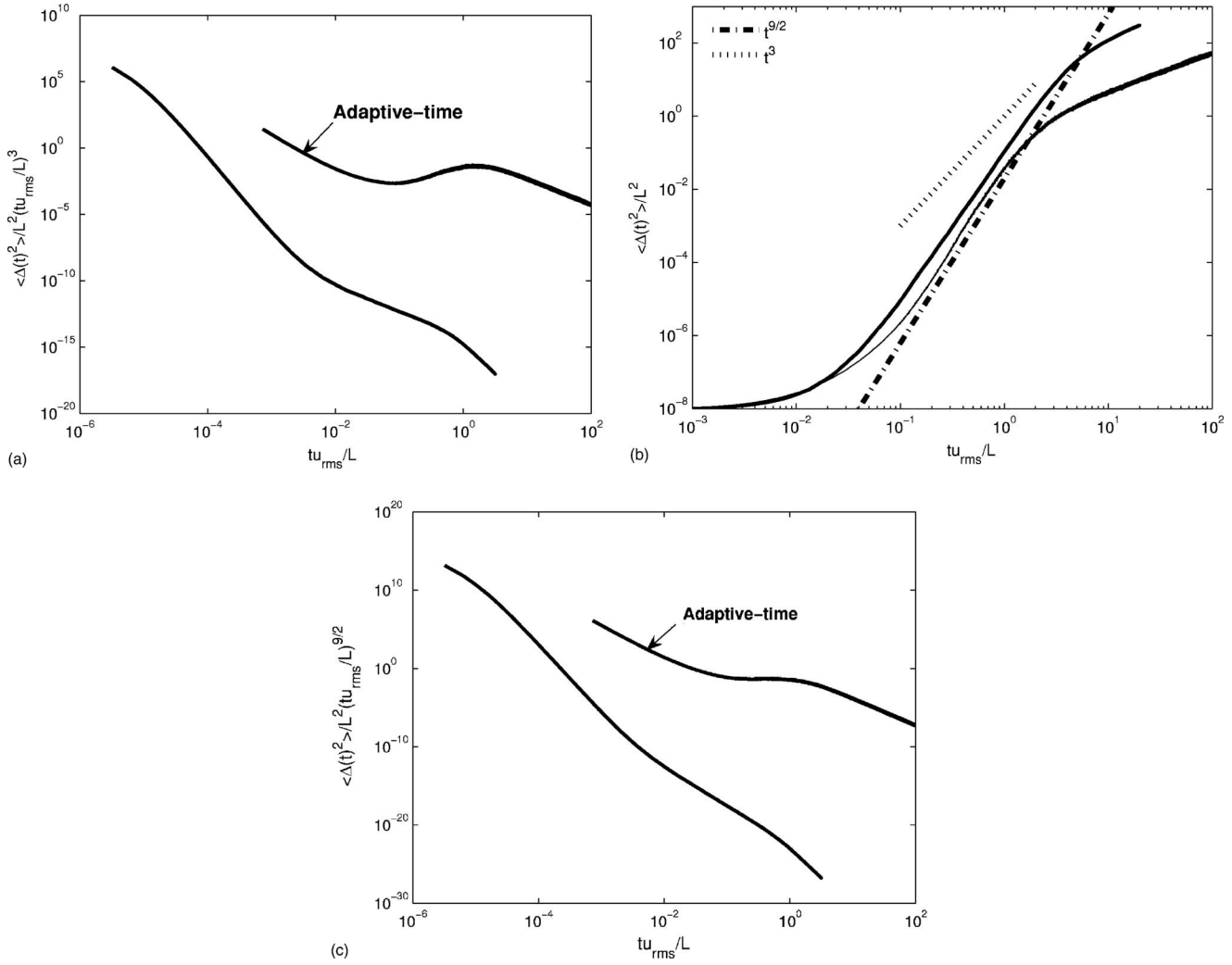

FIG. 4. Particle pair mean-square separation $\langle\Delta^2(t)\rangle$ normalized with the length scale $L=\frac{2\pi}{k_1}$. This simulation has the same initial conditions ($\Delta_0=0.1\eta$) and flow parameters as those used to produce Fig. 1 except we use an adaptive time step [15], $\Delta t=\min\left(C_1\frac{\min(\Delta,L)}{u_{rms}},C_2\frac{[\min(\Delta,L)]^{2/3}}{\lambda\epsilon^{1/3}}\right)$. We also plot for comparison, the curve $\langle\Delta^2(t)\rangle/L^2$ vs tu_{rms}/L of Fig. 1 (obtained with fully resolving constant time step). A clear $t^{9/2}$ scaling is observed in the case of the adaptive time step but not in the case of the constant time step. (a) $\langle\Delta^2(t)\rangle/L^2\left(\frac{tu_{rms}}{L}\right)^3$ vs tu_{rms}/L, (b) $\langle\Delta^2(t)\rangle/L$ vs tu_{rms}/L, (c) $\langle\Delta^2(t)\rangle/L^2\left(\frac{tu_{rms}}{L}\right)^{9/2}$ vs tu_{rms}/L.

The event can be thought of as a straining stagnation point; such a point in the flow is characterized by rapidly curving, divergent streamlines. Note that a scale, let us call it Δ_{ssp}, is associated with these stagnation points. This scale characterizes the spatial extent over which the curvature of the streamlines ending at or emanating from these stagnation points remains significantly correlated. For a separation event to be likely, Δ must be comparable to Δ_{ssp}. Since values of Δ_{ssp} exist over all scales due to the fractal nature of their distribution [13,22] this physical picture is very much in the spirit of the locality assumption of Ref. [1]. So, after n encounters with n stagnation points the separation becomes

$$\Delta_n=\rho_{ph}^n\Delta_0, \tag{27}$$

where ρ_{ph} is an actual physical property of the flow.

It is interesting to note that this picture of turbulent pair separations by discontinuous bursts can be formulated in terms of the "exit" time thresholds [35] where the average time $\langle T_\rho(\Delta)\rangle$ for a particle pair to pass from one threshold to another is determined. These exit times can be re-interpreted to be the average times taken for fluid element pairs with a separation of Δ to meet straining stagnation points with a characteristic length scale Δ_{ssp}, comparable to, or larger than, Δ and then suddenly burst to a separation $\rho\Delta$. The average distance between such straining stagnation points is approximately $n_s^{-1/d}\left(\frac{L}{\Delta}\right)$, where n_s is the number density of straining stagnation points [22] and d is the Euclidean dimension of the embedding space. According to Refs. [16,20]

$$n_s\left(\frac{L}{\Delta}\right)\approx C_sL^{-d}\left(\frac{L}{\Delta}\right)^{D_s}, \tag{28}$$

where C_s is a dimensionless constant of proportionality, and $D_s=\frac{d(3-p)}{2}$, where the wave-number energy spectrum is $E(k)\sim k^{-p}$ (in our present KS, $d=3$, $p=\frac{5}{3}$ and $D_s=2$) [22].

Reference [16] makes the assumption that, on average, fluid element pairs move with the rms velocity of the turbulence u_{rms} relative to stagnation points which remain statistically persistent in the flow in an appropriate inertial frame (see Sec. IV for a definition and analysis of this concept). Hence

$$\langle T_{\rho_{ph}}(\Delta)\rangle \sim \frac{n_s^{-1/d}\left(\frac{L}{\Delta}\right)}{u_{rms}} \sim \frac{L}{u_{rms}}\left(\frac{\Delta}{L}\right)^{D_s/d}. \tag{29}$$

Boffetta *et al.* [36] use the Richardson PDF equation to derive the exit times. However, Goto and Vassilicos [17] set out to derive a generalized PDF equation from their reinterpreted exit time [Eq. (29)]. They construct an equation for the rate of change of the probability, $Q_n(t)$, that a particle pair will be separated by a distance that is between Δ_n and Δ_{n+1} [see Eq. (27)],

$$\frac{d}{dt}Q_n = b_{n-1}Q_{n-1} - b_nQ_n. \tag{30}$$

The coefficient b_n must be proportional to the inverse of $\langle T_{\rho_{ph}}(\Delta_n)\rangle$ hence from Eq. (29)

$$b_n = B\frac{u_{rms}}{L}\left(\frac{\Delta_n}{L}\right)^{-g}, \tag{31}$$

where $g \equiv \frac{D_s}{d}$ and B is a dimensionless constant independent of Δ_n, u_{rms}, and L. Goto and Vassilicos [17] show that B depends on the proportionality constant C_s.

The relationship with the PDF of the pair separation is

$$Q_n(t) = \alpha\Delta_n P(\Delta_n, t), \tag{32}$$

where $\alpha \equiv \ln \rho_{ph}$. Goto and Vassilicos [17] argue that as long as the change in $Q_n(t)$ is small with the change in n then a Taylor expansion up to the second order is appropriate:

$$\frac{\partial P}{\partial t} = -B\alpha\frac{\partial}{\partial\Delta}(\Delta^{1-g}P) + \frac{B\alpha^2}{2}\frac{\partial}{\partial\Delta}\left(\Delta\frac{\partial}{\partial\Delta}(\Delta^{1-g}P)\right). \tag{33}$$

Imposing the initial condition of a vanishingly small separation and with some work, the solution of this equation is reached,

$$P(\Delta_n, t) = At^{-1/g}\left(\frac{\Delta^g}{\widetilde{B}g^2t}\right)^{1+2/\alpha g-1/g}\exp\left(-\frac{\Delta^g}{\widetilde{B}g^2t}\right), \tag{34}$$

where $A(g,\alpha)$ is a normalization factor and $\widetilde{B}$ replaces $\frac{B\alpha^2}{2}$.

This solution reduces to the self-similar form,

$$\widetilde{P}(\widetilde{\Delta}) = \widetilde{A}\widetilde{\Delta}^{2/\alpha-1+g}\exp\left(-G_0^{g/2}\widetilde{\Delta}^g\right), \tag{35}$$

where $\widetilde{P}(\widetilde{\Delta}) = \langle\Delta^2\rangle^{1/2}P(\Delta/\langle\Delta^2\rangle^{1/2})$, $\widetilde{A}(g,\alpha)$ is a normalization factor and

TABLE II. Run specification for pair separation PDF and related experiments. N_R is the number of KS flow field realizations and N_p is the number of sample trajectories per realization. The Kolmogorov time scale $t_\eta = \epsilon^{-1/3}k_\eta^{-2/3}$. The turbulent energy dissipation rate ϵ is determined by Eq. (13).

$k_1=\frac{2\pi}{L}$ $(2\pi\ \mathrm{m}^{-1})$	$k_\eta=\frac{2\pi}{\eta}$ $(2\pi\ \mathrm{m}^{-1})$	N_k	u_{rms} $(\mathrm{m\ s}^{-1})$	λ	Δt (s)	N_R	N_p
1.0	1000.0	100	1.0	0.5	$0.01t_\eta$	100	100

$$G_0 = \frac{\int_0^\infty x^{1+4/g\alpha+4/g}e^{-x^2}dx}{\int_0^\infty x^{1+4/g\alpha}e^{-x^2}dx}. \tag{36}$$

We attempt to fit Eq. (35) [with Eq. (36) taken into account] to PDFs obtained in a kinematic simulation whose flow parameters are detailed in Table II; the initial separation Δ_0 is prescribed as η and $\frac{L}{\eta}$ is set to 10^3 to facilitate faster computations. Following Ref. [20], we fix $g=\frac{D_s}{d}=\frac{2}{3}$. The results are shown in Fig. 5. A relatively conventional value of α, namely 1.5, is found to fit the data extremely well (leading to $\rho_{ph}\approx 4.48$ and $\alpha g=1$). This value is some way off the value of $\alpha=\frac{6}{7}$ required for Eq. (33) to exactly coincide with the Richardson PDF equation [1,17]. Nevertheless, KS reproduces the Richardson law, Eq. (1), and agrees with the self-similar collapse and form of the PDF [17] $P(\Delta,t)$. It is now important to investigate whether KS also agrees with the basic premise of this theory, namely, $\langle T_{\rho_{ph}}(\Delta)\rangle \sim \left(\frac{\Delta}{L}\right)^{2/3}$ (for $\frac{D_s}{d}=\frac{2}{3}$).

B. Time dependencies of pair separation statistics

In this section we define average travel time which, as we show, can be directly obtained from $P(\Delta,t)$, and then calculate exit times as differences between two average travel times. Taking a PDF approach to the problem, we can say that the probability that a particle pair's separation Δ is above a threshold Δ_n at time t is given by

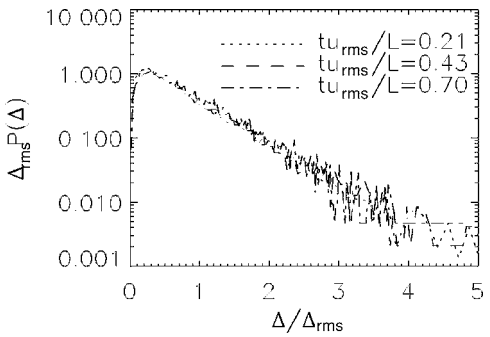

FIG. 5. Probability distribution functions for particle pair separation Δ. Flow parameters detailed in Table II; initial separation of fluid element pair $\Delta_0=\eta$; unsteadiness frequency, $\omega_n=\lambda\sqrt{k_n^3E(k_n)}$. The solid line is Eq. (35) using the values $\alpha=1.5$, $g=\frac{2}{3}$.

$$\int_{\Delta>\Delta_n} P(\Delta,t)d\Delta. \tag{37}$$

Similarly, the probability that a particle pair's separation Δ is above the threshold Δ_n after time $t+\delta t$ is

$$\int_{\Delta>\Delta_n} P(\Delta,t+\delta t)d\Delta. \tag{38}$$

The difference between the two probabilities [approximately $\delta t\int_{\Delta>\Delta_n}\frac{\partial}{\partial t}P(\Delta,t)d\Delta$ for small enough δt] represents the probability $p_{\Delta_n}(t)\delta t$ that a pair crosses Δ_n from below Δ_n between t and $t+\delta t$ minus the probability that the pair crosses Δ_n from above Δ_n at the same time. Assuming that the latter probability is negligible compared to $p_{\Delta_n}(t)\delta t$ [a reasonable assumption since $\langle\Delta^2(t)\rangle$ increases with time], we write

$$p_{\Delta_n}(t) \simeq -\int_{\Delta<\Delta_n}\frac{\partial}{\partial t}P(\Delta,t)d\Delta \tag{39}$$

(a similar formula is given in Ref. [33]). The average travel time for a particle pair's separation to reach Δ_n at t is then given by

$$\langle t\rangle_{\Delta_n} = \int_0^\infty dttp_{\Delta_n}(t) \tag{40}$$

so that one might expect

$$\langle T_\rho(\Delta_n)\rangle = \langle t\rangle_{\Delta_{n+1}} - \langle t\rangle_{\Delta_n}, \tag{41}$$

where $\Delta_{n+1}=\rho\Delta_n$. Note that if $\langle t\rangle_{\Delta_n}$ is a power law of Δ_n, then $\langle T_\rho(\Delta_n)\rangle$ is the same power law of Δ_n. Note also that we can define travel time moments for any power m as follows:

$$\langle t^m\rangle_{\Delta_n} = \int_0^\infty dtt^m p_{\Delta_n}(t). \tag{42}$$

Inserting Eq. (33) into Eq. (39) yields

$$p_{\Delta_n}(t) = B\alpha\Delta_n^{1-g}P(\Delta_n,t) - B\alpha\lim_{\Delta\to 0}[\Delta^{1-g}P(\Delta,t)] - \frac{B\alpha^2}{2}\Delta_n\frac{\partial}{\partial\Delta}[\Delta^{1-g}P(\Delta,t)]\Big|_{\Delta=\Delta_n} + \frac{B\alpha^2}{2}\lim_{\Delta\to 0}\Delta\frac{\partial}{\partial\Delta}[\Delta^{1-g}P(\Delta,t)]. \tag{43}$$

Using the similarity solution for the PDF equation [17] [Eq. (35)] we evaluate the second and fourth terms, respectively, finding they scale as $\Delta^{2/\alpha}$ and $\Delta^{2/\alpha+g}+\Delta^{2/\alpha}$, respectively. Therefore as long as $\alpha>1$ and $g>1$ and taking the limit $\Delta\to 0$, both terms are zero. Finally, substituting Eq. (34) into the two remaining terms we arrive at

$$p_{\Delta_n}(t) = \tilde{A}\exp(-G_0^{g/2}\tilde{\Delta}_n^g)\frac{\tilde{\Delta}_n^{2/\alpha}}{\sigma^g}\frac{B\alpha^2}{2}G_0^{g/2}\tilde{\Delta}_n^g. \tag{44}$$

Here, to alleviate notation, we use the definition $\tilde{\Delta}_n=\frac{\Delta_n}{\sigma}$ with $\sigma\equiv\langle\Delta^2\rangle^{1/2}$.

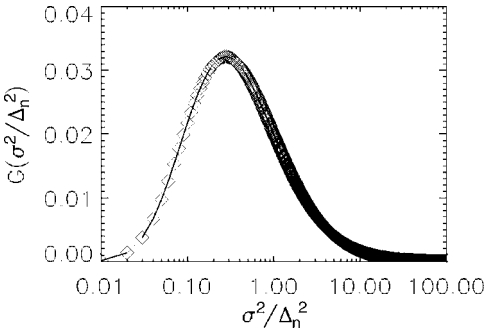

FIG. 6. Function $G(\tilde{\sigma}^2)$ is the kernel for integrating the root-mean square of the particle pair separation $t(\sigma^2)$, to obtain the average threshold travel time $\langle t^m_{\Delta_n}\rangle$. The function is only significant in the range $10^{-2}\lesssim\tilde{\sigma}^2\lesssim 10^1$.

Since all the time dependency is now contained in the standard deviation, i.e., $\sigma=\sigma(t)$, and this can be inverted so that $t=t(\sigma)$, we can define a change of variables

$$\tilde{\sigma}^2 \equiv \frac{\sigma^2}{\Delta_n^2}, \quad d\tilde{\sigma}^2 = 2\frac{\sigma\dot{\sigma}}{\Delta_n^2}dt. \tag{45}$$

Substituting Eq. (44) into Eq. (40) and using these changes in the variables we obtain

$$\langle t^m\rangle_{\Delta_n} = \tilde{A}\Delta_n^{-g}\int_0^\infty \frac{d\tilde{\sigma}^2}{(d/dt)\tilde{\sigma}^2(\tilde{\sigma}\Delta_n)}\exp(-G_0^{g/2}\tilde{\sigma}^{-g}) \times t^m(\tilde{\sigma}^2\Delta_n^2)\tilde{\sigma}^{-2g-2/\alpha}\frac{B\alpha^2}{2}G_0^{g/2}, \tag{46}$$

where m is the moment of the travel time. Note that the scaling of $\langle t^m\rangle_{\Delta_n}$ on Δ_n is independent of $\alpha\equiv\ln\rho$ if $t=t(\sigma^2)$ and $\sigma^2=\sigma^2(t)$ are well-defined power laws. In particular, α does not have to be equal to $\alpha_{ph}\equiv\ln\rho_{ph}$.

Disregarding the constants of proportionality since we are only interested in the scaling properties of the travel time moments,

$$\langle t^m\rangle_{\Delta_n} \sim \Delta_n^{-g}\int_0^\infty d\tilde{\sigma}^2 F(\tilde{\sigma}^2)\frac{t^m(\tilde{\sigma}^2\Delta_n^2)}{\frac{d}{dt}\tilde{\sigma}^2(\tilde{\sigma}\Delta_n)}, \tag{47}$$

where

$$F(\tilde{\sigma}^2) = \tilde{\sigma}^{-2g-2/\alpha}\exp(-G_0^{g/2}\tilde{\sigma}^{-g}). \tag{48}$$

Notice that $\frac{d}{dt}\tilde{\sigma}^2\sim\tilde{\sigma}^{2-g}\Delta_n^{-g}$ and we can now define a function $G(\tilde{\sigma}^2)$ that provides a kernel for the integration of the function $t(\sigma^2)$ to obtain the travel time moment,

$$\langle t^m\rangle_{\Delta_n} \sim \int_0^\infty d\tilde{\sigma}^2 G(\tilde{\sigma}^2)t^m(\tilde{\sigma}^2\Delta_n^2), \tag{49}$$

where

$$G(\tilde{\sigma}^2) = \frac{F(\tilde{\sigma}^2)}{\tilde{\sigma}^{2-g}} = (\tilde{\sigma}^2)^{-1-g/2-1/\alpha}\exp(-G_0^{g/2}(\tilde{\sigma}^2)^{-g/2}) \tag{50}$$

and is plotted in Fig. 6.

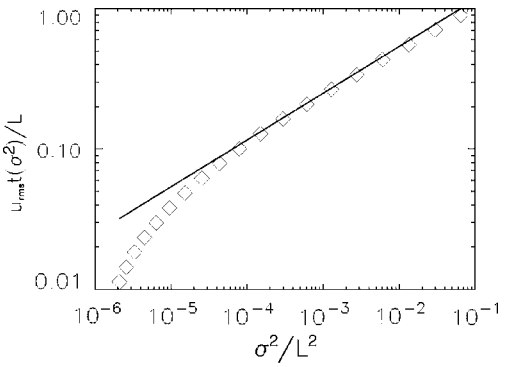

FIG. 7. Scaling of $\frac{u_{rms}t(\sigma^2)}{L}$ as a function of $\frac{\sigma^2}{L^2}$. Values of σ^2 are determined from PDFs of the separation of particle pairs at arbitrary times in a kinematic simulation used to produce Fig. 5 (i.e., $\Delta_0 = \eta$ and Table II). The solid line depicts the expected power law scaling, $t \sim (\sigma^2)^{1/3}$, which is observed for approximately two decades.

We can now deduce that if the scaling of σ^2 is a power law, i.e., $\sigma^2 \sim t^\gamma$, then the travel time moment $\langle t^m \rangle_{\Delta_n}$ should scale as

$$\langle t^m \rangle_{\Delta_n} \sim \Delta_n^{2m/\gamma}. \tag{51}$$

At this stage we need to verify the validity of the transformation [Eq. (49)] and the kernel [Eq. (50)] as they are based on the PDF equation of Ref. [16] and on the assumption that fluid element pairs cross thresholds Δ_n from below much more often than from above. We convolve the two functions $G(\tilde{\sigma}^2)$ and $t^m(\tilde{\sigma}^2\Delta_n^2)$ to obtain $\langle t^m \rangle_{\Delta_n}$ and compare the result with travel times directly calculated for both $m=1$ and $m=-1$. Use of Eq. (49) requires knowledge of $t(\sigma^2)$, which we plot in Fig. 7 using flow parameters identical to those used to produce Fig. 5. We define the scale factor of the convolution as $\Delta_n = \rho^n \Delta_0$. In this definition one can try any value $\rho > 1$, where ρ is not necessarily the physical multiplicative constant $\rho_{ph}=4.48$ of the straining stagnation point model described in the previous section. To aid faster computations we set the multiplicative factor ρ to 1.2 [37]. This does not preclude the possibility that the characteristic size of the multiplicative jump may, indeed, be a physical property of the flow (i.e., ρ_{ph}) since we have seen that the travel time scaling is independent of $\alpha = \ln \rho$ [Eq. (46)]. The results are shown in Fig. 8.

It is clear that the data produced by the convolution [Eq. (49)] are in good agreement with the directly determined travel times [the convolution data is truncated due to the lack of data for the long time $\tilde{\sigma}^2$ values needed for the limits of the integration of Eq. (49)] except at very small times where the neglect of initial conditions in Eq. (49) is evident. We also observe a Richardson-like scaling of $t(\sigma^2)^{1/3}$ over two decades of σ^2 in Fig. 7 as well as the corresponding power law, $\langle t^m \rangle_{\Delta_n} \sim \Delta^{2m/3}$ for $m = \pm 1$ in Fig. 8, confirming that the Richardson power-law scaling is valid. However, it is also noticeable that the power law $\langle t^m \rangle_{\Delta_n} \sim \Delta_n^{2m/3}$ is observed for a significantly smaller range than in Fig. 7. This is perhaps to be expected if we consider that the kernel [Eq. (50)] is non-

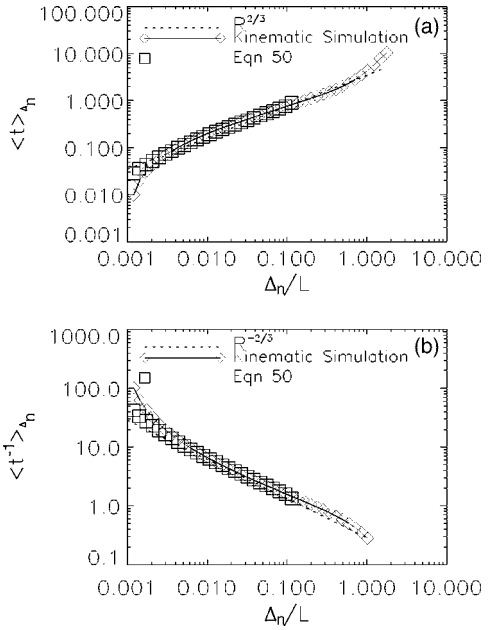

FIG. 8. Average travel time for a particle pair to separate from Δ_0 at $t=0$ to Δ_n. Initial conditions ($\Delta_0 = \eta$) and flow parameters are identical as those used to produce Fig. 5. Plots are for (a) $m=1$; (b) $m=-1$. Curves are tending towards a scaling of $\langle t^m \rangle_{\Delta_n} \sim \Delta_n^{2m/\gamma}$, where $\frac{2}{\gamma} = \frac{2}{3}$. Data determined from Eq. (49) agree with the directly calculated values.

zero only in the range $10^{-2} \lesssim \tilde{\sigma}^2 \lesssim 10^1$. So, if $G(\tilde{\sigma}^2)$ is convoluted with $t(\sigma^2)$ which has a power law, $t \sim \sigma^{2/\gamma}$, valid in the range $\sigma_{min} < \sigma < \sigma_{max}$ then the power law for the travel time, $\langle t^m \rangle_{\Delta_n} \sim \Delta_n^{2m/\gamma}$, will only be valid in the smaller range $\frac{10\sigma_{min}}{\sqrt{2}} < \Delta_n < \frac{\sigma_{max}}{\sqrt{10}}$.

From Eq. (41) and setting $m=1$ in Eq. (51) the exit time scales in the same way as $\langle t \rangle_{\Delta_n}$, i.e.,

$$\langle T_\rho(\Delta) \rangle \sim \Delta_n^{2/\gamma}. \tag{52}$$

We present results for the exit times $\langle T_\rho(\Delta) \rangle$ in Fig. 9 using identical flow parameters as those used to produce the travel times in Fig. 8. We use the definition of Ref. [32], that $\langle T_\rho(\Delta) \rangle$ is the average time required for fluid element pair

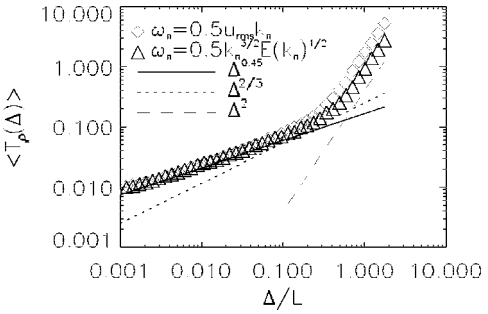

FIG. 9. Average exit times $\langle T_\rho(\Delta) \rangle$ for a fluid element pair to separate from one specified threshold Δ_n to another $\rho\Delta_n$. Flow parameters are detailed in Table II; $\Delta_0 = \eta$. No inertial-range power law corresponding to $g=\frac{2}{3}$ is observed for either $\omega_n = \lambda\sqrt{k_n^3 E(k_n)}$ or $\omega_n = \lambda u_{rms} k_n$. $g=\frac{4}{9}$ provides a better approximation.

separations to grow from Δ to $\rho\Delta$. We also use the two forms of time dependency to check in three-dimensional KS the assertion made by Ref. [13], for a two-dimensional form of the model, that the form of the time dependency does not significantly effect the scaling properties of pair dispersion. The first formulation is specified in Eq. (14) and the second in Eq. (15) and represents each scale of motion being swept by a single average velocity u_{rms}. Clearly the assumption of an average velocity neglects both the time dependency of the large-scale sweeping velocities and their direction. However, on average, this formulation, although incomplete and inaccurate, has been shown to go some way in representing the sweeping of the small-scale eddies by the large energy-containing ones [26].

It is clear from Fig. 9 that no regime of $\langle T_\rho(\Delta)\rangle \sim \Delta^{2/3}$ is observed; indeed one of $\langle T_\rho(\Delta)\rangle \sim \Delta^{4/9}$ might be a better fit. Considering that in this study we have shown the validity in kinematic simulation of Eq. (1) in Figs. 2 and 7, a tendency towards Richardson scaling in Fig. 8, and the validity of the PDF form [Eq. (35)] in Fig. 5, which implies $\gamma=\frac{2}{g}=3$, it is puzzling that the exit time diagnostic would not reveal signs of the same behavior. However, due to computational limitations, we have used a value of $\rho=1.2$ that is much smaller than the physical one, $\rho_{ph}=4.48$, that is supported by KS. In the context of the theory of Ref. [17], one might expect this diagnostic to reveal Richardson behavior most clearly when $\rho=\rho_{ph}$. It might be the case that the argument of Ref. [15] applies for a restricted range of early times and small separations (which can best be captured by the exit time diagnostic for small values of ρ) before Richardson behavior emerges. We leave the resolution of this puzzle for future study as clarifying scaling ranges will require much higher values of $\frac{L}{\eta}$. Such higher values are also required to accommodate the broader range of values of ρ needed, including ρ_{ph}. It is interesting to note that fluid element pair statistics obtained by Ref. [37] using DNS of isotropic turbulence exhibit much clearer Richardson scaling in the exit time statistics than in the direct pair separation statistics. We leave this issue for related future study as well.

IV. STATISTICAL PERSISTENCE HYPOTHESIS

In the previous section we presented evidence confirming Richardson scalings in kinematic simulation and showing that pair separation growth in KS is consistent with the picture where pairs travel together for a significant time and then separate suddenly when they encounter straining stagnation points in the turbulent flow. In this section we consider the conditions required for the validity of such a picture.

A. Stagnation point velocities

Since turbulence is a time dependent flow, stagnation points clearly do not remain stationary. Furthermore, they are not Galilean invariant. The underlying assumption in Refs. [17,22] is that there exists some frame of reference F_0 where the velocity streamline structure of the turbulence and hence the position of the stagnation points within that structure is, in some statistical sense, *persistent*. Goto and Vassilicos [17] call this the statistical persistence hypothesis (SPH), a concept which implies that stagnation points in frame F_0 can leave their imprint on pair diffusion statistics, leading, for example, to a PDF equation such as Eq. (33).

In any frame F the fluid velocity $u_i(\mathbf{x},t)$ vanishes at a stagnation point that has a position $\mathbf{x}=\mathbf{s}(t)$. This condition remains for as long as the stagnation point exists so that

$$\frac{d}{dt}u_i(\mathbf{s},t)=0. \tag{53}$$

Therefore we can define a velocity $\mathbf{V}_s \equiv \frac{d}{dt}\mathbf{s}(t)$ that describes the motion of the stagnation point, and

$$\frac{\partial u_i(\mathbf{s},t)}{\partial t} = -\mathbf{V}_s \cdot \nabla u_i(\mathbf{s},t). \tag{54}$$

By definition, the fluid acceleration is

$$a_i = \frac{\partial u_i}{\partial t} + \mathbf{u}\cdot\nabla u_i \tag{55}$$

and at $\mathbf{x}(t)=\mathbf{s}(t)$ where $u_i=0$, it therefore follows from Eqs. (54) and (55) that

$$a_i = -\mathbf{V}_s \cdot \nabla u_i. \tag{56}$$

This relation is kinematic and valid in any frame of reference F. The solution of Eq. (56) is given via Cramer's rule,

$$\mathbf{V}_s = -\frac{[\det(\mathbf{a},\partial_2\mathbf{u},\partial_3\mathbf{u}),\det(\partial_1\mathbf{u},\mathbf{a},\partial_3\mathbf{u}),\det(\partial_1\mathbf{u},\partial_2\mathbf{u},\mathbf{a})]}{\det(\partial_1\mathbf{u},\partial_2\mathbf{u},\partial_3\mathbf{u})}, \tag{57}$$

where $\partial_j=\frac{\partial}{\partial x_j}$. This allows us to forgo the complicated process of not only finding a stagnation point in the flow but then following it in a Lagrangian sense through a time-dependent flow field. Indeed, only a snapshot of the flow field is necessary to determine the stagnation point velocities with Eq. (57).

From Eq. (56) it follows that the root-mean-square values of the acceleration and stagnation point velocity are related by

$$a' \sim V_s' \frac{u_\eta}{\eta} \tag{58}$$

since we expect the spatial derivative of the velocity to be dominated by the smallest scales (any dashed quantity in the remainder of the paper will denote an rms quantity although we keep u_{rms} instead of u' for consistency with the rest of this study). In Eq. (58), a' is calculated by averaging over all stagnation points in frame F and is therefore equal to the root-mean-square a_l' of the local acceleration $\mathbf{a}_l \equiv \frac{\partial}{\partial t}\mathbf{u}$ (we also define the convective acceleration $\mathbf{a}_c \equiv \mathbf{u}\cdot\nabla\mathbf{u}$). Later in this section we verify in kinematic simulation the validity of Eq. (58) with a' replaced by a_l' and also test whether Eq. (58) remains valid if a' is calculated by averaging over the entire flow. If we assume the small scale velocity scaling [4] $u_\eta \sim (\epsilon\eta)^{1/3}$ and the associated scaling $\epsilon \sim \frac{u_{rms}^3}{L}$, then

$$\frac{La_l'}{u_{rms}^2} \sim \left(\frac{V_s'}{u_{rms}}\right)\left(\frac{L}{\eta}\right)^{2/3}, \tag{59}$$

where the acceleration variance has been normalized with the large scales.

In KS homogeneous isotropic turbulence where large scale sweeping of small scales is absent, we might expect Kolmogorov [4] scaling for a_l', i.e. $a_l' \sim \frac{u_\eta^2}{\eta}$, which implies

$$\frac{La_l'}{u_{rms}^2} \sim \left(\frac{L}{\eta}\right)^{1/3}. \tag{60}$$

It then follows that

$$\frac{V_s'}{u_{rms}} \sim \left(\frac{L}{\eta}\right)^{-1/3}. \tag{61}$$

The negative scaling of $\frac{V_s'}{u_{rms}}$ implies that, in a statistical sense, the movement of the stagnation points becomes less significant when compared with the movement of the fluid elements of the flow (i.e., the movement characterized by u_{rms}) as the Reynolds number increases. In this way, the stagnation points become more persistent in time and space allowing the fluid element pairs to "feel" the imprint of this coherent (persistent) stagnation point structure on their statistics. DNS experiments [38,18] agree with the concept of increasing stagnation point persistence as both studies report $\frac{La'}{u_{rms}^2} \sim \left(\frac{L}{\eta}\right)^{1/2}$ which may be some way from the scaling predicted by application of Ref. [4] but is consistent with the DNS result [18] $\frac{V_s'}{u_{rms}} \sim \left(\frac{L}{\eta}\right)^{-1/6}$ which also implies increasing stagnation point persistence with increasing Reynolds number.

B. Persistence of stagnation points in kinematic simulation

Of course the persistence of these stagnation points and the statistical persistence hypothesis can only be established if a frame exists where $\langle \mathbf{V}_s \rangle$ (the averaging operation $\langle \cdots \rangle$ is taken over all stagnation points in the relevant frame of reference) is small enough (ideally zero). It is in such a frame that we can argue that persistence of stagnation points increases as $\frac{L}{\eta}$ increases on account of

$$\frac{V_s'}{u_{rms}} \sim \left(\frac{L}{\eta}\right)^{q}, \tag{62}$$

with $q<0$ ($q=-\frac{1}{3}$ for Ref. [4], $q=-\frac{1}{6}$ for current DNS). DNS evidence [18] suggests that $\langle \mathbf{V}_s \rangle = 0$ is the frame F_0 where the mean flow is zero, i.e., where $\langle \mathbf{u} \rangle = 0$ (the averaging operation $\langle \cdots \rangle$ is taken over all space or, equivalently, over all realizations since the turbulence is considered homogeneous). The DNS evidence [18] also suggests that F_0 is the only frame where $\langle \mathbf{V}_s \rangle = 0$, and that $\langle \mathbf{V}_s \rangle$ is, in general, proportional to the relative velocity between any frame F and frame F_0.

Figure 10 presents examples of PDFs of $\mathbf{V}_s$ in frame F_0 obtained by kinematic simulations with flow parameters detailed in Table III over a wide range of inertial-range extent and with a variety of time-dependency formulations. Sampling took place over a fixed volume L_V^3 where L_V is the largest scale involved in the largest inertial range simulated. Each simulation consisted of 5×10^6 random initial starting points for a Newton-Rhapson algorithm searching for the stagnation points hence leading to an average distance between starting points of approximately 6η. Many realizations of the flow field were used so that the wave-vector orientations have an approximately uniform distribution ($N_R N_k \sim 1 \times 10^6$). Clearly, Fig. 10 shows that the assumption that $\langle V_{s_i} \rangle = 0$ over the flow domain in F_0 is a valid one. Note that when $\lambda = 0$ then $\mathbf{V}_s \equiv 0$ at all stagnation points in F_0 because $\frac{\partial u_i}{\partial t} \equiv 0$.

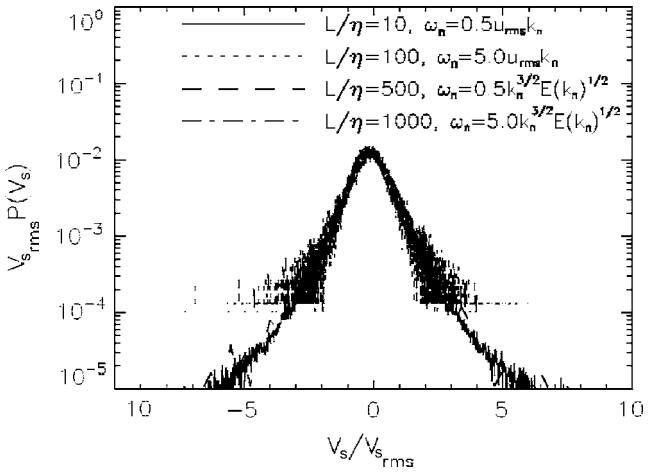

FIG. 10. Example PDFs of the stagnation point velocity V_{s_i}. In these simulations η remains fixed while L is increased to control the size of the inertial range (see Table III). Although there is variation in the range of V_{s_i}, the PDFs all scale with the rms of the stagnation point velocity in a similar way.

The SPH claims that there is a frame where the persistence is maximized. To investigate the behavior of the stagnation points in other frames of reference F we investigate the average accelerations conditional on the velocity $\mathbf{U}$ of the reference frame with respect to F_0. With acceleration being Galilean invariant, accelerations at stagnation points in F are the same as accelerations at points where $\mathbf{u}=\mathbf{U}$ in F_0. Hence average accelerations conditional on $\mathbf{u}=\mathbf{U}$ in F_0, $\langle \mathbf{a} | \mathbf{U} \rangle$, are equal to $-\langle \mathbf{V}_s \cdot \nabla \mathbf{u} \rangle$, where the average is taken over all stagnation points in frame F. Kinematic simulations for $\frac{L}{\eta}=10$, 100, 1000 with persistence parameters $\lambda=0$, 0.5, 5.0 using the time-dependency formulations from Eqs. (14) and (15) all lead to $\langle a_i | \mathbf{u} \rangle = 0$ for any $\mathbf{u}$. This implies that in any frame F $\langle \mathbf{V}_s \cdot \nabla \mathbf{u} \rangle = 0$ and therefore $\mathbf{V}_s$ and $\nabla \mathbf{u}$ are uncorrelated in KS.

These results, and in particular the result $\langle a_i | \mathbf{u} \rangle = 0$ which underpins them, are perhaps to be expected when one con-

TABLE III. Run specification for stagnation point velocity experiments. N_R is the number of KS flow field realizations and N_s is the number of starting points for the Newton-Rhapson algorithm per realization.

$k_\eta = \frac{2\pi}{\eta}$ (2π m^{-1})	N_K	u_{rms} (m s^{-1})	N_R	N_s
1000.0	100	1.0	10000	500

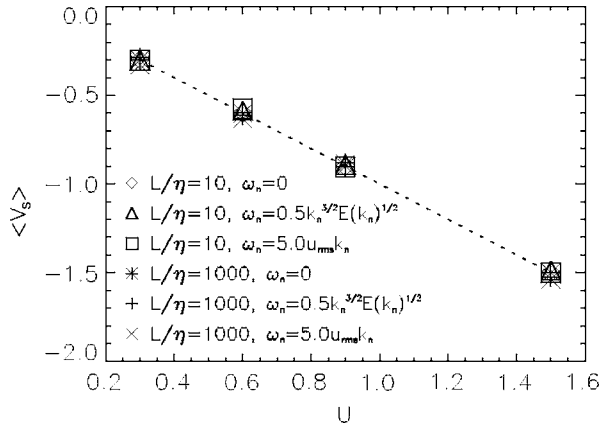

FIG. 11. Average stagnation point velocity $\langle V_s \rangle$ in frame moving with velocity $(U,0,0)$. Flow parameters are detailed in Table III. In a statistical sense the stagnation points move in the opposite direction to the frame of reference with velocity $-(U,0,0)$.

siders the lack of dynamics and the related lack of Fourier mode interactions in kinematic simulation. Unlike DNS [18], which includes the dynamics of turbulence, kinematic simulations have no mechanism for generating any coherent restoring accelerations that are anti-correlated with the velocity (i.e., a large velocity that is associated with a large acceleration in the opposite direction).

The KS results of Fig. 11 show that $\langle \mathbf{V}_s \rangle = -\mathbf{U}$ in frame F for many values of $\frac{L}{\eta}$ and λ. We have also confirmed that Fig. 11 remains the same for either formulation of $\omega_n(k_n)$. Hence the statistical persistence is maximized at stagnation points in F_0 where $\langle \mathbf{V}_s \rangle = 0$, and this statistical persistence improves as $\frac{L}{\eta} \to \infty$ due to $\frac{V_s'}{u_{rms}} \sim \left(\frac{L}{\eta}\right)^q$ with $q < 0$.

C. Acceleration scalings

Taking advantage of kinematic simulation's ability to impose an arbitrary form of energy spectrum on the flow, we can reformulate Eq. (59) into more general forms using the scaling $u_\eta \sim u_{rms}\left(\frac{\eta}{L}\right)^{(p-1)/2}$, which follows from $E(k) \sim u_{rms}^2 L(kL)^{-p}$;

$$\frac{La_l'}{u_{rms}^2} \sim \left(\frac{V_s'}{u_{rms}}\right)\left(\frac{L}{\eta}\right)^{(3-p)/2}. \tag{63}$$

Similarly, the Kolmogorov scaling in Eq. (60) can be generalized on the basis of $a_l' \sim \frac{u_\eta^2}{\eta}$ to give

$$\frac{La_l'}{u_{rms}^2} \sim \left(\frac{L}{\eta}\right)^{2-p}. \tag{64}$$

Having split the acceleration into a local component, $\mathbf{a}_l = \frac{\partial}{\partial t}\mathbf{u}$, and a convective component [39], $\mathbf{a}_c = \mathbf{u}\cdot\nabla\mathbf{u}$, we calculate both components in frame F_0 using the KS velocity field and its derivatives.

The results for the scalings of the root-mean-square values of the local and convective accelerations, respectively, a_l' (averages taken over all space generate same scaling as averages taken over stagnation points only) and a_c' (averages taken over all space) can be seen in Fig. 12. The first point of interest in the figure is that the scaling of the rms convective acceleration component is

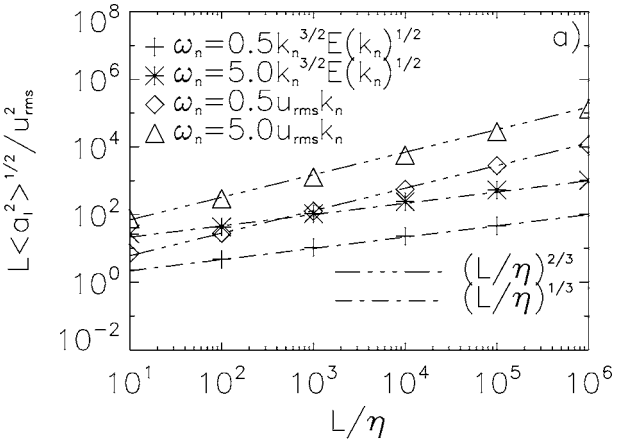

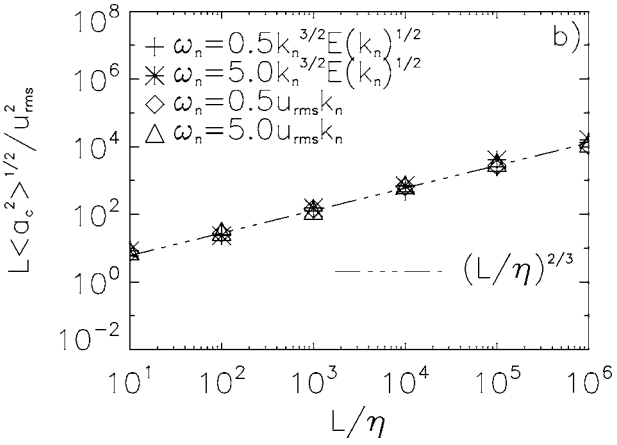

FIG. 12. Scaling with $\frac{L}{\eta}$ of the rms values of (a) the local acceleration component a_l, and (b) the convective acceleration component a_c. Flow parameters are detailed in Table IV. The convective component is independent of the time dependency of the flow and the scaling is universal for all simulations. Both the local acceleration component's strength and scaling behavior depend on the time dependency of the flow.

$$\frac{La_c'}{u_{rms}^2} \sim \left(\frac{L}{\eta}\right)^{(3-p)/2} \tag{65}$$

regardless of the time dependency of the turbulent field [see Fig. 12(b)]. This can be understood as it follows from $a_c' \sim u' \frac{u_\eta}{\eta}$ which holds in KS because of its lack of sweeping.

In contrast, the rms of the local acceleration a_l' depends very much on the formulation of $\omega_n(k_n)$, since it scales as

$$\frac{La_l'}{u_{rms}^2} \sim \left(\frac{L}{\eta}\right)^{2-p} \tag{66}$$

when the unsteadiness frequency is determined by Eq. (14) yet scales in an identical way to the convective component, i.e.,

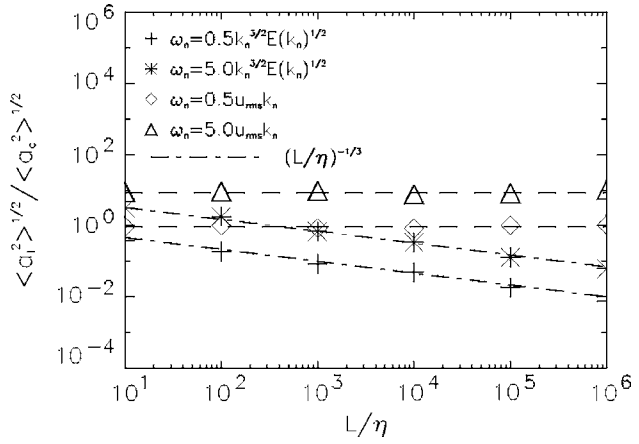

FIG. 13. Scaling with $\frac{L}{\eta}$ of the ratio between the rms values of the local acceleration component a_l, and the convective acceleration component a_c. Flow parameters are detailed in Table IV. The behavior is similar to that of $\frac{V_s'}{u_{rms}}$ observed in Fig. 15.

$$\frac{La_l'}{u_{rms}^2} \sim \left(\frac{L}{\eta}\right)^{(3-p)/2}, \tag{67}$$

when Eq. (15) is used.

As a result it is the relative strength of the local component to the convective component, $\frac{a_l'}{a_c'}$, that ultimately determines the scaling of $a'^2=a_l'^2+a_c'^2$ in KS. It is clear from Figs. 12 and 13 that a_c' dominates a_l' when $\omega_n \sim k_n^{2/3}$ and $\lambda=0.5$ even at modest values of $\frac{L}{\eta}$. However, when $\lambda=5.0$, a_c' does not begin to dominate a_l' until $\frac{L}{\eta}>10^3$, which explains the deviation of the total acceleration variance from a scaling of $\frac{La'^2}{u_{rms}^2} \sim \left(\frac{L}{\eta}\right)^{(3-p)/2}$ towards a more Kolmogorov-like scaling for $\frac{L}{\eta} \lesssim 10^3$ in Fig. 14 where we plot the scaling of the total acceleration variances (obtained from averages over the entire flow) for various values of the imposed energy spectrum

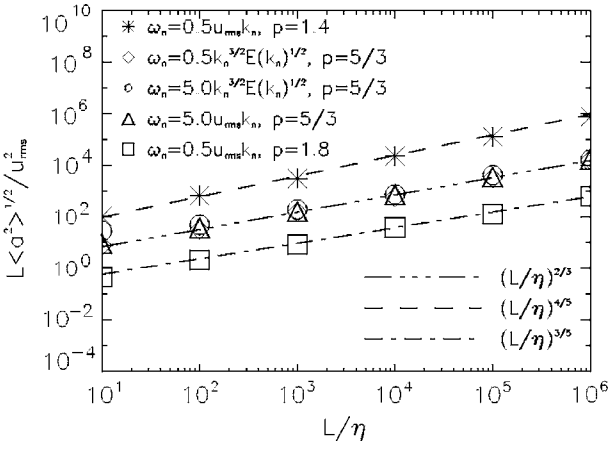

FIG. 14. Scaling of rms acceleration a' normalized with the large scales. Flow parameters detailed in Table IV. The scaling $\frac{3-p}{2}$ is observed for all values of the energy spectrum exponent p and for all models of unsteadiness frequency except for $\omega_n=5.0\sqrt{k_n^3E(k_n)}$ when $\frac{L}{\eta} \lesssim 10^3$. Data for $p=\frac{5}{3}$ are brought together in the interests of clarity.

TABLE IV. Run specification for stagnation point velocity experiments. N_R is the number of KS flow field realizations and N_a is the number of random sampling points per realization.

$k_\eta=\frac{2\pi}{\eta}(2\pi\ \mathrm{m}^{-1})$	N_K	u_{rms} (m s^{-1})	N_R	N_a
1000.0	100	1.0	1	10^6

exponent p and both models of unsteadiness frequency ω_n. The common flow parameters are detailed in Table IV. Clearly, the scaling $\frac{La'}{u_{rms}^2} \sim \left(\frac{L}{\eta}\right)^{(3-p)/2}$ is observed rather than of the Kolmogorov-type scaling, $\frac{La'}{u_{rms}^2} \sim \left(\frac{L}{\eta}\right)^{2-p}$ for all the simulations except for a deviation at values of $\frac{L}{\eta} \lesssim 10^3$ when $\omega_n=5.0\sqrt{k_n^3E(k_n)}$.

Direct numerical simulation of isotropic turbulence [39] have shown that $\mathbf{a}_l$ and the solenoidal part of $\mathbf{a}_c$ are approximately equal but antialigned in F_0. Referring to Figs. 12 and 13 it is clear that no such tendency exists in kinematic simulation since $a' \gtrsim a_c'$. This adds to the argument above regarding the lack of dynamics in kinematic simulation, but also suggests that Kolmogorov scaling of a' seems to be closely related to the antialignment of $\mathbf{a}_l$ and the solenoidal part of $\mathbf{a}_c$.

D. Statistical persistence

We directly determine the scaling of $\frac{V_s'}{u_{rms}}$ using flow parameters in Table III and Fig. 15 depicts the behavior with increasing $\frac{L}{\eta}$.

It is clear from Fig. 15 that in the cases where the pseudosweeping time dependency [Eq. (15)] is implemented in kinematic simulation, the scaling agrees with Eqs. (63) and (67) i.e., $q=0$ and $\frac{V_s'}{u_{rms}}=c$ where c is a dimensionless constant dependent on, and in fact increasing with, λ. When it is Eq. (14) that is used to determine the time dependency of KS, the results seem to indicate that q takes to the Kolmogorov value, $q=-\frac{1}{3}$ in agreement with Eqs. (63) and (66). Let us make the important point that with $q=0$ in our KS, the statistical persistence of stagnation points is measured by c and is a direct reflection of the persistence parameter as $c \propto \lambda$. In spite of q being different from the Kolmogorov value $q=-\frac{1}{3}$, Richardson scalings are observed in kinematic simulation (as reported in this paper) only for small values of λ [13,22], thus confirming the view that Richardson scaling requires some statistical persistence of stagnation points to be realized [17].

In investigating the source of the scalings found in Fig. 15, we can make a relatively trivial observation for the case where $\omega_n(k_n)=\lambda u_{rms}k_n$. In these simulations the velocity stagnation points move with the large scale velocity (and not relative to each other) so that

$$V_s' \sim \frac{\omega_n(k_n)}{k_n} \sim \lambda u_{rms}. \tag{68}$$

Therefore the scaling does not depend on the length scale and c is proportional to λ as we indeed observe (see Fig. 15).

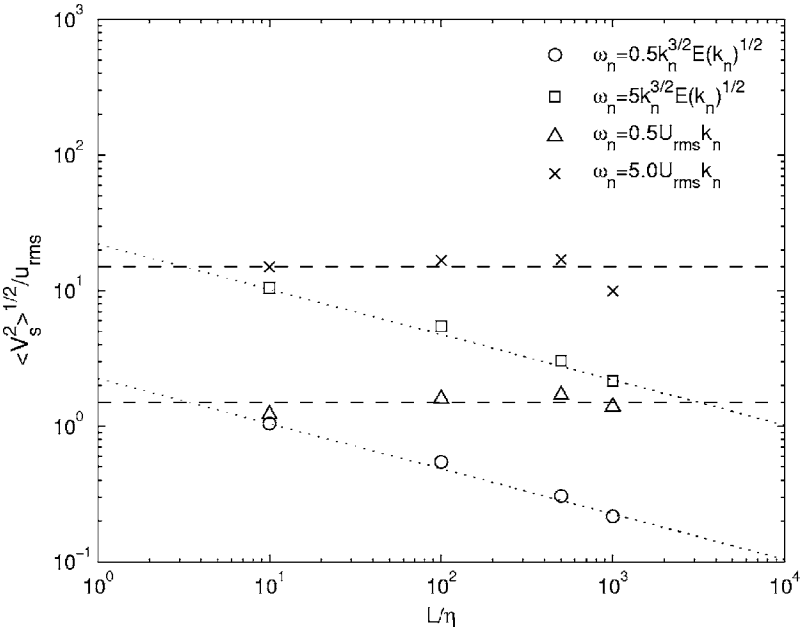

FIG. 15. Scaling of the rms values of the stagnation point velocity V_s' with $\frac{L}{\eta}$. Flow parameters detailed in Table III. The two dotted lines correspond to $\left(\frac{L}{\eta}\right)^{-1/3}$. The two dashed lines correspond to $\left(\frac{L}{\eta}\right)^{0}$.

For small enough values of λ, the proportionality constant $c(\lambda)<1.0$, thus supporting SPH in kinematic simulation with $\omega_n(k_n)=\lambda u_{rms}k_n$ for small values of λ, i.e., that the motion of the stagnation points is statistically insignificant compared to the characteristic motion of the fluid. If we apply the same reasoning to the simulations where $\omega_n=\lambda\sqrt{k_n^3E(k_n)}$, even though the modes may be moving in complex ways relative to each other, we find that the rms velocity of stagnation points related to length scales $\frac{2\pi}{k}$ is given by $\frac{\omega_n(k_n)}{k_n}\sim k_n^{-1/3}$. It is therefore reasonable to expect that V_s' (where all stagnation points are taken into account) is dominated by $k_{N_K}=\frac{2\pi}{\eta}$, and therefore

$$\frac{V_s'}{u_{rms}}\sim\left(\frac{L}{\eta}\right)^{-1/3}. \tag{69}$$

This scaling is also observed in our KS (see Fig. 15) and supports SPH in kinematic simulation with $\omega_n(k_n)=\lambda\sqrt{k_n^3E(k_n)}$.

E. Lifetime of stagnation points

The lifetime of stagnation points is also crucial to the statistical persistence hypothesis. For the theory to be valid, not only must the stagnation points become more persistent in space as the Reynolds number increases, but they must also be persistent in time, i.e., they must exist for long enough times. The lifetime of stagnation points must be determined by the time that it takes for one stagnation point to meet another, since such a meeting seems to be the only mechanism by which stagnation points can be destroyed.

Any stagnation point can be thought of as having a "sphere of influence" surrounding them which is defined by a characteristic length Δ_{ssp} over which the curvature of the streamlines that emanate from it remain correlated. From Eq. (28) (in the case $p=\frac{5}{3}$, $D_s=2$, and $d=3$), the average distance separating two stagnation points associated with the length scale Δ_{ssp} is

$$\left[n_s\left(\frac{L}{\Delta ssp}\right)\right]^{-1/d}\sim L\left(\frac{\Delta_{ssp}}{L}\right)^{2/3}. \tag{70}$$

We can therefore calculate a time $t_{ssp}(\Delta_{ssp})$ for stagnation points of size Δ_{ssp} approaching each other head-on as the ratio of the average distance given by Eq. (70) to the characteristic velocity of such stagnation points, i.e.,

$$t_{ssp}(\Delta ssp)=\frac{\left[n_s\left(\frac{L}{\Delta ssp}\right)\right]^{-1/d}}{u_{rms}\left(\frac{\Delta_{ssp}}{L}\right)^{1/3}}. \tag{71}$$

However, most of the time stagnation points will miss each other, so the average lifetime of stagnation points must also involve the probability that stagnation points may collide. This probability $p\left(\frac{\Delta_{ssp}}{L}\right)$ is proportional to $\left(\frac{\Delta_{ssp}}{L}\right)^d n_s\left(\frac{\Delta_{ssp}}{L}\right)$, which scales as $\left(\frac{\Delta_{ssp}}{L}\right)^{3-2}$ in the present case ($d=3$, $D_s=2$). The average lifetime of a stagnation point is

$$T_{ssp}=\int_{\eta/L}^{1}t_{ssp}(\Delta_{ssp})p\left(\frac{\Delta_{ssp}}{L}\right)d\left(\frac{\Delta_{ssp}}{L}\right). \tag{72}$$

Substituting into Eq. (72),

$$T_{ssp}\sim\int_{\eta/L}^{1}\frac{L}{u_{rms}}\left(\frac{\Delta_{ssp}}{L}\right)^{1/3}\left(\frac{\Delta_{ssp}}{L}\right)d\left(\frac{\Delta_{ssp}}{L}\right), \tag{73}$$

and integrating we finally arrive at the average lifetime of a stagnation point,

$$T_{ssp}\sim\frac{L}{u_{rms}}. \tag{74}$$

That stagnation points essentially last as long as the flow realization (if we think of a new realization of the field starting at $\frac{L}{u_{rms}}$ intervals) is entirely consistent with the notion that the persistent-in-space (and now -in-time) stagnation point

field is distributed in such a way that determines the scaling of the mean-square separation to be of the Richardson [1] form as the Reynolds number increases.

V. SUMMARY AND CONCLUSIONS

The fundamental process of the behavior of two fluid elements separating in a kinematically simulated field has been investigated. Initially, direct calculations of the separation statistics are studied. Later, an approach based on the streamline topology of the turbulent flow field [13,17,22] is used.

Following from the uncertainty of previous studies [13,14,15] as to kinematic simulation's ability to reproduce the temporal scaling of the fluid element pair's separation, $\langle\Delta^2(t)\rangle \sim t^3$, predicted by Ref. [1], we determine that the temporal scaling for an initial separation Δ_0 significantly smaller than η in our KS to be neither Richardson-like nor as predicted by Ref. [15] based on arguments citing the lack of small-scale eddy advection in kinematic simulation. We follow the advice of Ref. [14] and directly determine the mean diffusivity, $\frac{d}{dt}\langle\Delta^2(t)\rangle$, to minimize the effects of the initial conditions. We find that KS does, indeed, reproduce Richardson's diffusion prediction $\frac{d}{dt}\langle\Delta^2(t)\rangle \sim \Delta^{4/3}$ over a wide range of scales and with much less dependence on Δ_0, and not the diffusivity predicted by Ref. [15] of $\frac{d}{dt}\langle\Delta^2(t)\rangle \sim \Delta^{14/9}$. Furthermore, we show that the adaptive integration time step used by Thomson and Devenish [15] favors the temporal scaling $\langle\Delta^2(t)\rangle \sim t^{9/2}$.

The validity in kinematic simulation of the generalized self-similar solution to the PDF equation of the pair separation [17], $\widetilde{P}(\widetilde{\Delta})$, derived from the concept of velocity stagnation points [13,22] is tested. Good agreement is found in the case where its variance σ^2 obeys Richardson scaling.

The time dependencies of the pair separation statistics are investigated. We establish a relationship between the average travel time $\langle t^m\rangle_{\Delta_n}$ of a pair's separation to a threshold Δ_n and the inverse function of the temporal evolution of the rms separation $t(\sigma^2)$. This relationship shows good agreement with directly calculated values. The function $t(\sigma^2)$ can be made to scale in a Richardson-like fashion for approximately two decades with a careful choice of the initial separation, $\Delta_0 = \eta$. This is in contrast to the choice of Δ_0 (significantly smaller than η) when determining $\langle\Delta^2(t)\rangle$, which led to anomalous scaling. We show that due to the nature of the finite range of the integration kernel $G(\widetilde{\sigma}^2)$, the travel times $\langle t^m\rangle_{\Delta_n}$ exhibit very short ranges of Richardson power law behavior. The exit times $\langle T(\Delta_n)\rangle$ are shown to exhibit power-law behavior different to Richardson scaling.

The concept of straining stagnation points is explored further and a mathematical formulation of the statistical persistence hypothesis [17] (SPH) is introduced using exact kinematic relations (see also Ref. [17]). We show that in KS, in the frame F_0 where the mean-fluid velocity is zero, the persistence of straining stagnation points is maximized and SPH is valid. In further testing the validity of the SPH in kinematic simulation, we find that the total acceleration variance scales as $\frac{La'}{u_{rms}^2} \sim \left(\frac{L}{\eta}\right)^{(3-p)/2}$ rather than $\frac{La'}{u_{rms}^2} \sim \left(\frac{L}{\eta}\right)^{2-p}$ [for $E(k) \sim k^{-p}$] except in the case where $\omega_n = 5.0\sqrt{k_n^3 E(k_n)}$ and $\frac{L}{\eta} \lesssim 10^3$. By splitting the acceleration variance into local a_l' and convective a_c' components we find that the single case of deviation from $\frac{La'}{u_{rms}^2} \sim \left(\frac{L}{\eta}\right)^{(3-p)/2}$ at moderate values of $\frac{L}{\eta}$ is caused by the local component of the acceleration a_l' which scales à la Kolmogorov when $\omega_n \sim \sqrt{k_n^3 E(k_n)}$, dominating the convective component a_c' which always scales as $\frac{La_c'}{u_{rms}^2} \sim \left(\frac{L}{\eta}\right)^{(3-p)/2}$. We show that for small values of λ the reverse is true and when $\omega_n \sim u_{rms} k_n$ both components scale as $\frac{La_l'}{u_{rms}^2} \sim \frac{La_c'}{u_{rms}^2} \sim \left(\frac{L}{\eta}\right)^{(3-p)/2}$. Finally, we present an argument which shows that the mean lifetime of stagnation points scales with the integral time scale of the turbulence.

ACKNOWLEDGMENTS

D. R. Osborne and J. C. Vassilicos acknowledge support from the UK Natural Environment Research Council and the Royal Society of London, respectively.

[1] L. F. Richardson, Proc. R. Soc. London, Ser. A **110**, 709 (1926).
[2] A. M. Obukhov, Izv. Akad. Nauk SSSR, Ser. Geogr. Geofiz. **4**(4-5), 453 (1941).
[3] G. K. Batchelor, Q. J. R. Meteorol. Soc. **75**, 133 (1950).
[4] A. N. Kolmogorov, Dokl. Akad. Nauk SSSR **30**, 301 (1941).
[5] M.-C. Jullien, J. Paret, and P. Tabeling, Phys. Rev. Lett. **82**, 2872 (1999).
[6] S. Ott and J. Mann, J. Fluid Mech. **422**, 207 (2000).
[7] J. Paret and P. Tabeling, Phys. Rev. Lett. **79**, 4162 (1997).
[8] P. K. Yeung, Phys. Fluids **6**, 3116 (1994).
[9] P. K. Yeung and M. S. Borgas, J. Fluid Mech. **503**, 93 (2004).
[10] M. S. Borgas and P. K. Yeung, J. Fluid Mech. **503**, 125 (2004).
[11] T. Ishihara and Y. Kaneda, Phys. Fluids **14**, L69 (2002).
[12] G. Boffetta, A. Celani, A. Crisanti, and A. Vulpiani, Phys. Rev. E **60**, 6734 (1999).
[13] J. C. Fung and J. C. Vassilicos, Phys. Rev. E **57**, 1677 (1998).
[14] F. Nicolleau and G. Yu, Phys. Fluids **16**, 2309 (2004).
[15] D. J. Thomson and B. J. Devenish, J. Fluid Mech. **526**, 277 (2005).
[16] M. K. Rivera and R. E. Ecke, Phys. Rev. Lett. **95**, 194503 (2005).
[17] S. Goto and J. C. Vassilicos, New J. Phys. **6**, 65 (2004).
[18] S. Goto, D. R. Osborne, J. C. Vassilicos, and J. D. Haigh, Phys. Rev. E **71**, 015301(R) (2005).
[19] M. A. I. Khan, A. Pumir, and J. C. Vassilicos, Phys. Rev. E **62**, R1 (2000).
[20] P. Flohr and J. C. Vassilicos, J. Fluid Mech. **407**, 315 (2000).
[21] N. A. Malik and J. C. Vassilicos, Phys. Fluids **11**, 1572 (1999).
[22] J. Davila and J. C. Vassilicos, Phys. Rev. Lett. **91**, 144501

(2003).
[23] M. A. I. Khan and J. C. Vassilicos, Phys. Fluids **16**, 216 (2004).
[24] S. B. Pope, *Turbulent Flows* (Cambridge University Press, Cambridge, England, 2000).
[25] H. Tennekes, J. Fluid Mech. **67**, 561 (1975).
[26] D. R. Osborne, J. C. Vassilicos, and J. D. Haigh, Phys. Fluids **17**, 035104 (2005).
[27] A. S. Monin and A. M. Yaglom, *Statistical Fluid Mechanics* (MIT Press, Cambridge, MA, 1971).
[28] F. Nicolleau and J. C. Vassilicos, Phys. Rev. Lett. **90**, 024503 (2003).
[29] B. L. Sawford, P. K. Yeung, M. S. Borgas, and P. Vedula, Phys. Fluids **15**, 3478 (2004).
[30] G. A. Voth, A. La Porta, A. M. Crawford, J. Alexander, and E. Bodenschatz, J. Fluid Mech. **469**, 121 (2002).
[31] N. Mordant, P. Metz, O. Michel, and J.-F. Pinton, Phys. Rev. Lett. **87**, 214501 (2001).
[32] N. Mordant, J. Delour, E. Léveque, A. Arnéodo, and J.-F. Pinton, Phys. Rev. Lett. **89**, 254502 (2002).
[33] J. Jiménez, A. A. Wray, P. G. Saffman, and R. S. Rogallo, J. Fluid Mech. **255**, 65 (1993).
[34] J. C. Fung, J. C. R. Hunt, N. A. Malik, and R. J. Perkins, J. Fluid Mech. **236**, 281 (1992).
[35] G. Boffetta, A. Celani, A. Crisanti, and A. Vulpiani, Europhys. Lett. **46**, 177 (1999).
[36] G. Boffetta and I. Solokov, Phys. Fluids **14**, 3224 (2002).
[37] G. Boffetta and I. Solokov, Phys. Rev. Lett. **88**, 094501 (2002).
[38] P. Vedula and P. K. Yeung, Phys. Fluids **11**, 1208 (1999).
[39] A. Tsinober, P. Vedula, and P. K. Yeung, Phys. Fluids **13**, 1974 (2001).